

Multiscale Coupling in Function Space - Weak Coupling Between Molecular Dynamics and Continuum Mechanics

Konstantin Fackeldey ^{*} Rolf Krause[†]

We present a function space oriented coupling approach for the multiscale simulation of nonlinear processes in mechanics using finite elements and molecular dynamics concurrently. The key idea is to construct a transfer operator between the different scales on the basis of weighted local averaging instead of using point wise taken values. The local weight functions are constructed by assigning a partition of unity to the molecular degrees of freedom (Shepard's approach). This allows for decomposing the micro scale displacements into a low frequency and a high frequency part by means of a weighted L^2 -projection. Numerical experiments illustrating the stabilizing effect of our coupling approach are given.

Keywords:

multiscale, molecular dynamics, weak coupling, partition of unity method, mortar

1 Introduction

Multiscale modelling allows for the concurrent description of material properties and behavior on different scales. Often, two scales are considered, a small scale (micro scale) and a larger scale (macro scale). The micro scale is designed to capture the material properties on the molecular or atomistic level, whereas the macro scale is connected to a continuous description. Processes taking place on the atomistic level as, e.g., fracture, can therefore be incorporated into the macro model without changing the continuous description significantly. For the numerical simulation of multiscale models often molecular dynamics on the atomistic scale and finite elements on the continuous scale are

^{*}Institute for Numerical Simulation, University of Bonn Wegelerstraße 6, 53115 Bonn (Germany) (fackeldey@ins.uni-bonn.de).

[†]Institute for Numerical Simulation, University of Bonn Wegelerstraße 6, 53115 Bonn (Germany) (krause@ins.uni-bonn.de).

employed. It is a central aim of multiscale methods to provide systematic techniques for an accurate coupling between the respective atomistic and continuous models.

For example, within the Quasi-Continuum Method [1], following the Cauchy-Born rule, the scale transfer is realized by clustering degrees of freedom on the micro scale and identifying particular representative atoms with nodes of the finite element mesh.

Other widely used techniques are up-scaling methods [2, 3, 4] and concurrent coupling schemes [2, 5, 1, 6, 7, 8, 9, 10]. Up scaling methods derive a macroscopic model from a microscopic model by using, e.g., asymptotic expansions or Taylor expansions. In contrast, the coupling schemes employ the micro and macro model concurrently and impose additional constraints on both scales in order to enforce the coupling conditions.

For example, the bridging scale method [11, 12, 13] is a multiscale method by means of which the solution is decomposed into a micro scale and a macro scale part. The displacements on the macro scale are obtained by minimizing the error between the molecular dynamics displacements and the finite element displacements in a least-squares sense.

The bridging domain method [7, 8] and the Atomistic to Continuum (AtC) method [14, 15, 16] use a coupling region which is only a portion of the continuum and the molecular domain. In the bridging domain method the energy in the continuum atomistic overlap region is given by a convex combination of the continuum and atomistic contributions. In the AtC coupling the overlap region is used to impose the constraints between the continuum and atomistic solution in a weak sense. In [16] four classes of AtC blending methods providing a mathematical framework for the coupling of atomistic and continuum models are established. In [15] the AtC method for blending the continuum stress and the atomistic force is applied to a hierarchical structure consisting of a linear elastic, a non-linear elastic and an EAM-based atomistic model.

In order to gain computational efficiency, often the microscopic discretization is applied only in small regions of interest, where it either replaces or enriches the macro scale. When following this approach, one major problem are spurious boundary reflections or photon reflections at the boundary of the molecular dynamics domain.

One cause of this spurious boundary modes can be found in the fact that the atomistic scale contains high frequency information that cannot be represented by means of the discretization on the macro scale. Therefore high frequency waves might be reflected instead of propagated into the coarse scale. This phenomenon has already been observed in the mid seventies by Adelman and Doll [17]. The methods used to overcome this difficulty depend on the coupling method employed. For a detailed description of these reflection in the context of the Quasi Continuum Method we refer to the overview article of Curtin and Miller [9].

Also, non-reflecting boundary techniques, which are boundary conditions, that reduce the amount of the spurious reflections, were developed in connection with wave equations [18] and can be adopted to the multiscale setting [17, 19, 12, 3]. They find their application, for instance, on the context of wave propagation phenomena on unbounded domains, in order to make the computational domain finite. These boundary conditions cannot be found in a unified manner since they are also called e.g. absorbing, transparent, open one way or free-space boundary conditions.

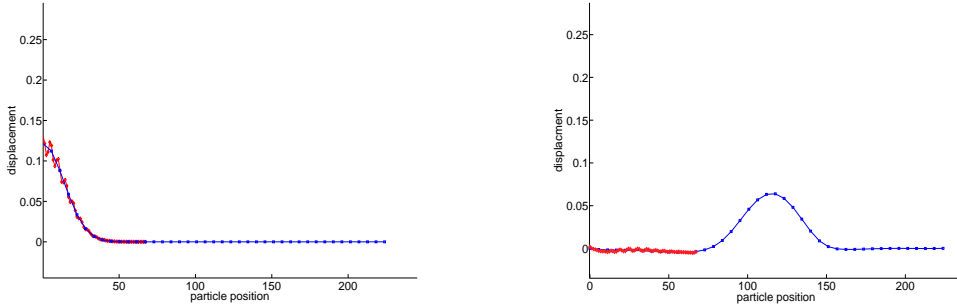


Figure 1: *left: starting configuration with initial amplitude, right: spurious reflections are damped*

In [12], the boundary reflections are eliminated by introducing forces to atoms close to the interface. These forces are equivalent to the lattice impedance. However, these damping techniques use a time history kernel which involves inverse Laplace transformation in time and Fourier transformation in space. This requires a global problem on the interface to be solved which is numerically costly. An example of damping in order to eliminate reflections is shown in Figure 1 where we applied Berenger’s concept of perfectly matched boundary layer [20, 21].

Here we present a new transfer operator based on a weak coupling approach. The key idea is to construct the transfer operator on the basis of weighted local averaging instead of using point wise taken values as in [7, 22, 11, 13]. Moreover, the continuum description overlaps the complete molecular domain, thus we have no handshake or blending region. The local weight functions are constructed by assigning a partition of unity to the molecular degrees of freedom. This allows for decomposing the micro scale displacements into a low frequency and a high frequency part by means of a weighted L^2 -projection. Thus, the entire formulation is in the setting of a function space.

Since our operator is based on a weak formulation of the transfer conditions with respect to the L^2 -scalar product, quadrature is necessary for the assembling of its algebraic representation. For a detailed description of the related data-structures and methods we refer to [23], where a similar quadrature problem in the context of non-linear contact problems is treated.

Of course, the transfer of physical quantities such as temperature or stress, between different scales, is a demanding task. For recent approaches we refer to [44, 45, 46]. In [44] an equivalent continuum for a dynamically deforming atomistic particle system is defined. The equivalence is among other achieved by interpreting the mechanical stress as an internal force, which interacts between material points. In [45] a review of local thermomechanical quantities obtained from molecular dynamic simulations is given. An other approach for the construction of a local atomic deformation gradient [46] might also be applicable to our new coupling scheme.

This paper is structured as follows. In Section 2 we briefly introduce the fine scale setting and the coarse scale setting. The separation of the displacement field into a coarse scale part and a fine scale part is shown in Section 3. In Section 4, the new

coupling approach is presented. Applications can be found in the last section.

2 Multiscale Modeling

Let us consider a body $\Omega \subset \mathbb{R}^d$, $d = 1, 2, 3$, which, under the influence of external and internal forces, will undergo some deformation. In this section, we give a multiscale approach for the description of the body's deformation. This multiscale approach is based on the concurrent usage of molecular dynamics (MD), which is associated to the micro scale, and finite elements (FE), which are associated to the macro scale. Since this type of coupled multiscale simulation requires a thorough information transfer between the micro and the macro scale, we begin our considerations by describing in more detail the discrete models used on the respective scales.

Let us start with the micro scale. For reasons of computational efficiency, the MD-simulation is only applied locally to a portion $\Omega' \subset \Omega$ of our body. This domain of interest Ω' might be the neighborhood around a crack tip or at the vicinity of a contact boundary, where local effects are expected to take place which cannot be represented on the coarser scale. In the remaining part $\Omega \setminus \Omega'$ only the coarse scale model will be employed. The material behavior on the micro scale is now modelled by means of an isolated system of atoms or molecules of a crystalline solid. We identify each of the atoms in their reference position with a point $X_\alpha \in \mathbb{R}^d$, $\alpha \in \mathcal{A}$, where \mathcal{A} is an index set. Under the influence of external and internal forces, the atoms displace in space. The position \hat{X}_α from the α -th atom in a deformed configuration is then given as

$$\hat{X}_\alpha = X_\alpha + q_\alpha, \quad (1)$$

where q_α is the displacement of atom α .

The atomic displacements $q = (q_\alpha)_{\alpha \in \mathcal{A}}$ are assumed to obey Newton's law of motion

$$M_A \ddot{q} = f^{\text{internal}} + f^{\text{external}}, \quad (2)$$

where f^{internal} and f^{external} are the internal and external forces. With each atom α , we associate the mass $m_\alpha > 0$, such that

$$M_A = \text{diag}(m_\alpha \text{Id}_{\mathbb{R}^{d \times d}})_{\alpha \in \mathcal{A}} \quad (3)$$

is the mass matrix on the micro scale. In case a potential V is given, the internal forces acting on a conservative system can be obtained as $f^{\text{internal}} = -\nabla_{\hat{X}} V(\hat{X})$.

Summing up for each configuration stemming from (1), the state of the α th particle is given by

$$(X_\alpha, q_\alpha) \in \mathbb{R}^d \times \mathbb{R}^d \quad (4)$$

The finite element model employed on the macro scale is based on a continuum mechanics approximation of the deformation of our body Ω . Following the basic approach of continuum mechanics, on the macro scale the body in its reference configuration is

identified with the smooth and bounded domain $\Omega \subset \mathbb{R}^d$. The deformed configuration of Ω is given by $\phi(\Omega)$, where

$$\phi: \Omega \longrightarrow \mathbb{R}^d \quad (5)$$

is the deformation mapping and

$$u = \phi - \text{id} \quad (6)$$

are the displacements, see, e.g., [24]. Let us emphasize that in contrast to the micro scale description (1), each point of Ω is now associated with a material point in Ω .

In order to approximate the continuous displacement field u , we now employ a finite element discretization of lower order. Let \mathcal{T}^h denote a shape regular mesh with mesh size parameter $h > 0$ which approximates Ω . We use Lagrangian conforming finite elements of first order (P_1) for the displacements u and denote the set of all nodes of \mathcal{T}^h by \mathcal{N}^h . The finite element space $\mathcal{S}^h(\Omega) \subset H^1(\Omega)$ is spanned by the nodal basis

$$\mathcal{S}^h(\Omega) = \text{span}_{p \in \mathcal{N}^h} \{\lambda_p^h\}.$$

The Lagrangian basis functions $\lambda_p^h \in \mathcal{S}^h$ are uniquely characterized by the Kronecker-delta property

$$\lambda_p^h(q) = \delta_{pq}, \quad p, q \in \mathcal{N}^h,$$

where δ_{pq} is the Kronecker-delta. Any function $\bar{u} \in \mathcal{S}^h(\Omega)$ can uniquely be written as

$$\bar{u} = \sum_{p \in \mathcal{N}^h} \bar{u}_p \lambda_p^h, \quad (7)$$

where $(\bar{u}_p)_{p \in \mathcal{N}^h} \in \mathbb{R}^{d \cdot |\mathcal{N}^h|}$, $\bar{u}_p \in \mathbb{R}^d$, is the coefficient vector. We can identify each element of $\mathcal{S}^h(\Omega)$ with its coefficient vector $(\bar{u}_p)_{p \in \mathcal{N}^h}$. In a next step we define the subset $\Omega' \subset \Omega$ where the the coarse as well as the fine scale simulation is present. To do so, we define $\mathcal{T}_*^h \subset \mathcal{T}^h$ as the set of simplexes having a nonempty intersection with the particles, i.e.,

$$\mathcal{T}_*^h = \{T \in \mathcal{T}^h, \exists X_\alpha, \alpha \in \mathcal{A} : X_\alpha \in T\}.$$

Thus we have

$$\Omega' = \bigcup_{T \in \mathcal{T}_*^h} T, \quad \mathcal{S}_*^h = \mathcal{S}^h(\Omega)|_{\Omega'}, \quad \text{and} \quad \mathcal{N}_*^h = \mathcal{N}^h \cap \Omega'.$$

Let us remark that the size and shape of the domain Ω' is not given a priori and can be chosen arbitrarily.

Here, we do not incorporate any Dirichlet boundary conditions into the ansatz-space $\mathcal{S}^h(\Omega)$, since the finite element space $\mathcal{S}^h(\Omega)$ will only serve as the coarse scale space for the representation of the total displacement field. In order to simplify our notation, in the forthcoming we omit the superscript h whenever possible. Throughout this paper, we denote nodes by Latin letters, e.g., p, s, t, \dots and atoms by Greek letters, e.g., α, β, \dots

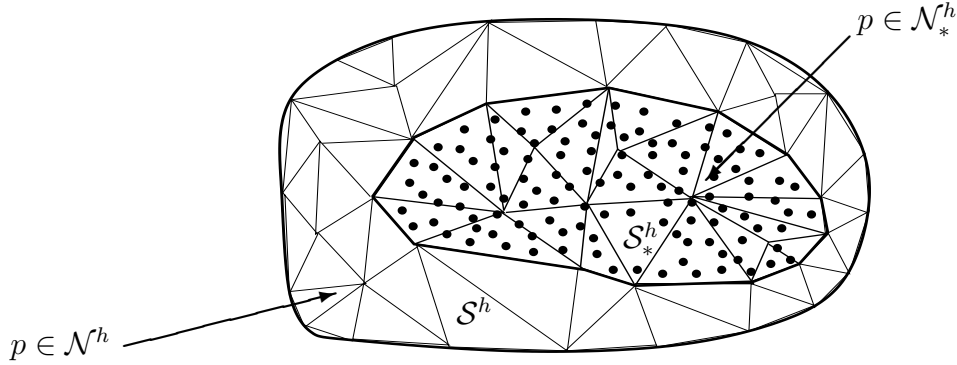


Figure 2: *The finite element space S^h and its restriction to Ω'*

3 Multiscale Decompositions

Since the length scales of the coarse scale and the fine scale differ by orders of magnitudes, it is natural to decompose the total displacement field into a coarse scale and a fine scale part. Taking into account the different maximal frequencies which can be represented by the respective discretization, we can decompose the total displacement field w into a low oscillatory part \bar{w} and a high oscillatory part w' ,

$$w = \bar{w} + w', \tag{8}$$

see Figure 3 for an illustration. This kind of scale-decomposition has been used in the context of bridging scale methods [11] and of variational multiscale methods [25]. The decomposition (8), however, requires that w' as well as \bar{w} are elements of the same vector space. In [11], the Euclidean space is chosen, whereas the variational multiscale

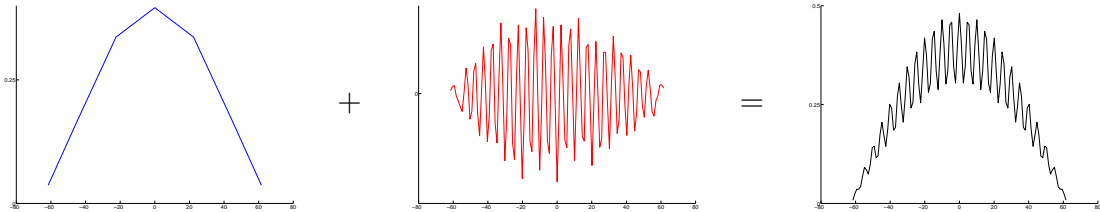


Figure 3: *Scale decomposition of the total displacement field w*

decomposition [25] relies on conforming finite element spaces which are used on the respective scales. In the following we propose a decomposition in an L^2 sense within an infinite-dimensional function space.

4 Weak Multiscale Coupling

In this section we present our new coupling operator for the information transfer between the molecular dynamics model (fine scale) and the continuum mechanics model (coarse

scale). The coupling between the different length scales is usually done in a fully discrete framework, see [1, 22, 11, 7]: after discretizing the continuum mechanics by, e.g., finite elements, the coarse scale solution is interpreted as an element of the Euclidean space. Then, the transfer is realized by the identification of point values [1] or by means of a least-squares approach [26, 22, 11].

Here, we propose a different approach, where the construction of the transfer operator takes advantage of an infinite dimensional function space. This is motivated by the stabilizing effect of weak coupling operators in the context of non-conforming domain decomposition or mortar methods for elliptic problems, see, e.g., [27, 28, 29]. There, for the transfer of displacements and stresses between non-matching meshes or different discretizations, a discrete L^2 -projection instead of an interpolation operator is used. Similar to mortar methods, our coupling approach is non-symmetric in the sense that one scale (the “slave” scale) inherits the values for the displacements from the other scale (the “master” scale). It is a particular advantage of the weak coupling approach that it provides a stable coupling independent of the respective mesh sizes. This feature is of crucial importance for multiscale simulations, since the employed length scales differ in orders of magnitude.

4.1 Design of Local Approximation Spaces

The L^2 -projection used for the scale transfer, introduced informally above, is formulated in a function space based setting. Thus the decomposition given by (8) should also be in the function space. However, in the molecular dynamics simulation, each molecule is an element of \mathbb{R}^d . Therefore we use an approximation, which maps the discrete displacement of the atoms $q_\alpha, \alpha \in \mathcal{A}$ into a function space, i.e.

$$\iota : (\mathbb{R}^d \times \mathbb{R}^d)^{|\mathcal{A}|} \rightarrow L^2(\Omega') \quad \iota(X, q) = w.$$

In order to interpret a molecular displacement as a function in L^2 , we employ local approximation spaces for each atom as it is done in the context of Partition of Unity methods (PUM) [30, 31, 32].

The starting point for our PUM is to build an approximation space V^{PUM} . To do so, a patch $\omega_\alpha \in \mathbb{R}^d$ is attached to each point, such that the union of these patches form an open cover $C_\omega := \{\omega_\alpha\}_{\alpha \in \mathcal{A}}$ of the domain. To this end, we define for each atom α a patch ω_α associated with $X_\alpha \in \Omega'$ as

$$\omega_\alpha = \{x \in \mathbb{R}^d : \|X_\alpha - x\| < h_\alpha\}.$$

The most basic property, which these patches have to fulfill, is that they cover the complete domain Ω' :

$$\bigcup_{\alpha \in \mathcal{A}} \omega_\alpha \supset \Omega'.$$

For an example of a 2D sketch see Figures of 4. On the basis of such a suitable cover C_ω we can define a partition of unity via data fitting techniques. In general, the term data fitting method refers to the construction of special shape functions φ_i for the

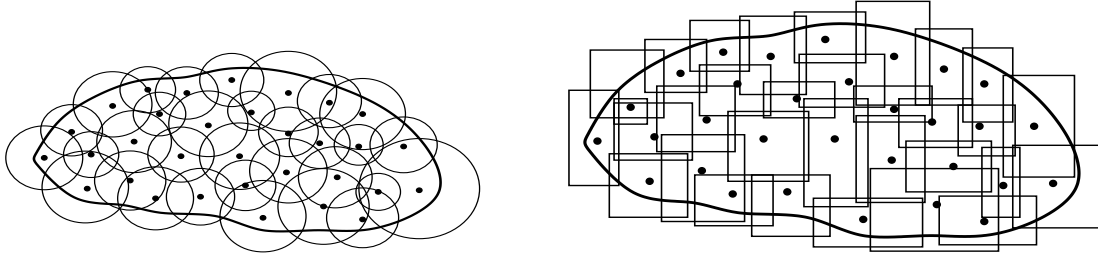


Figure 4: *Left*: A domain with circular patches. *Right*: A domain with rectangular patches

approximation of some function u from a discrete data set \mathcal{D} . The approximation u^S is then given by

$$u^S(x) := \sum_{i=1}^{|\mathcal{D}|} u_i \varphi_i(x),$$

where the u_i are given data.

Here, we follow Shepard's approach [33] for the construction of a PU. Thus, the shape functions φ_α are defined as

$$\varphi_\alpha(x) = \frac{W_\alpha(x)}{\sum_\beta W_\beta(x)}, \quad (9)$$

with weight functions W_α . Shepard [33] originally proposed the use of

$$W_\alpha(x) = \|x - X_\alpha\|^{-t}, \quad t > 0, \quad x \in \Omega. \quad (10)$$

It can easily be seen that the weight functions defined in (10) have a global support and therefore the functions φ_α have also a global support. Consequently, the evaluation of one shape function involves all weight functions W_β . Hence a localized version of Shepard's Method should be employed to ensure the compact support of φ_α , i.e. we assume $\text{supp}(W_\alpha) = \bar{\omega}_\alpha$ so that

$$\varphi_\alpha(x) = \frac{W_\alpha(x)}{\sum_{\omega_\beta \in \{\omega_\gamma : \omega_\gamma \cap \omega_\alpha \neq \emptyset\}} W_\beta(x)}, \quad x \in \omega_\alpha.$$

Thus w from (8) can be given by

$$w := \iota(X, q) = \sum_{\alpha=1}^{|\mathcal{A}|} q_\alpha \varphi_\alpha(x). \quad (11)$$

Besides the support of the W_α , the smoothness of the weight functions directly influences the smoothness of the shape functions. Here, we use Splines as weight functions [32]. For more details concerning the approximation properties of the PUM we refer to [30].

Most of the approximation techniques for the construction of shape functions, use a Moving Least Squares (MLS) approach, originated from scattered data approximation. In the MLS method one wishes to find the best approximation from a certain approximation space to the data at a some point x with respect to a weighted l_2 inner product. Moreover, the Shepard functions only reproduce the constant and hence, they have approximation order one in L^2 . We remark that our coupling operator does not depend on the construction of the shape functions via Shepard's approach (0th order MLS). However, other moving least squares method like higher order MLS, e.g. [34], Reproducing Kernel Particle Methods (RKPM)[35, 36, 37] or Radial Basis Functions (RBF)[38, 39] can be used.

4.2 Weak Multiscale Operator

In this section we derive a new approach for the coupling between molecular dynamics (fine scale) and continuum mechanics (coarse scale). Our approach is based on ideas from non-conforming domain decomposition methods, namely mortar methods. The key ideas of mortar methods is to provide a stable coupling between different discretizations or meshes by means of using a weak continuity condition at the respective interfaces. Starting from linear problems [27], mortar methods have been extensively studied in the context of elliptic partial differential equations, see, e.g. [28] and the references cited therein.

In the context of multiscale simulations, however, the coupling is often realized by means of the interpolation operator, since the molecules are in general interpreted as points in R^d , see, e.g., [22, 12]. Unfortunately, this might lead to undesirable effects due to the insufficient representation of the high frequency components of the fine scale solution by finite element functions. Using the techniques described in the previous Section, however, we are free to interpret atoms either as elements in \mathbb{R}^d or as functions in L^2 . Assuming that the masses are unity, this allows for a function space based coupling, leading to our weak multiscale operator.

Our aim is to construct a coarse scale approximation $\bar{w} \in \mathcal{S}^h$ of the total displacement function given by (11). The coarse scale representation $\bar{w} \in \mathcal{S}^h$ of the molecular displacement function w is defined by means of the L^2 -projection $\pi^h: L^2(\Omega') \rightarrow \mathcal{S}_*^h$, i.e.

$$\pi^h(w) \in \mathcal{S}_*^h : (\pi^h(w), \mu)_{L^2(\Omega')} = (w, \mu)_{L^2(\Omega')} \quad \forall \mu \in M^h, \quad (12)$$

where, the multiplier space M^h is defined by

$$M^h = \text{span}\{\mu_s \mid s \in \mathcal{N}_*^h\}.$$

Here, the basis functions μ_s , $s \in \mathcal{N}_*^h$ are assumed to have the local support $\text{supp}\mu_s \subseteq \text{supp}\lambda_s|_{\overline{\Omega'}}$. As is the case in the mortar setting, there are several possible choices for the basis functions μ_s of M^h . We follow the standard approach, see, e.g. [27, 28] by setting

$$\mu_s = \lambda_s|_{\overline{\Omega'}}, \quad s \in \mathcal{N}_*^h. \quad (13)$$

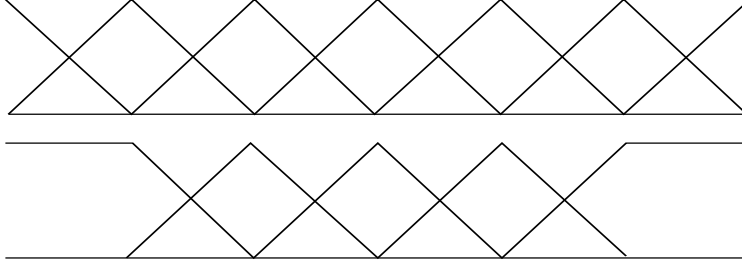


Figure 5: *Upper: Lagrange Multiplier Space M^h , lower: Lagrange Multiplier Space M_{mod}^h*

As an alternative, the multiplier space can also be given by

$$M_{mod}^h = \{\mu \mid \mu \in \mathcal{S}_*^h, \mu|_T \in P_0(T) \text{ if } T \cap \partial\Omega' \neq \emptyset\}. \quad (14)$$

In this modified multiplier space, the order of a test function is reduced by one if it contains an endpoint of \mathcal{S}_*^h (see Figure 5). In this case, we have to modify \mathcal{S}_*^h by imposing homogeneous Dirichlet boundary condition. Let us remark that the choice of the multiplier space M^h reflects the way \bar{w} is extended into \mathcal{S}^h .

Our coarse scale representation is now defined by extending $\pi^h(w) \in \mathcal{S}_*^h$ to \bar{w} , i.e. $\bar{w} = \mathcal{E}(\pi^h(w))$, where $\mathcal{E} : \mathcal{S}_*^h \rightarrow \mathcal{S}^h$ is an extension operator. Thus we can rewrite (8) by

$$w = w' + \bar{w} = (w - \mathcal{E}(\pi^h(w))) + \mathcal{E}(\pi^h(w)). \quad (15)$$

For the extension operator \mathcal{E} , different choices are possible cf. [40]. Here we chose

$$\mathcal{E}(v) = \sum_{p \in \mathcal{N}^h} v_p \lambda_p \text{ with } \begin{cases} v_p = w_p & , \quad p \in \mathcal{N}_*^h, \\ v_p = 0 & , \quad \text{else.} \end{cases}$$

As a consequence of our choice (13) of the multiplier space, the displacements in \mathcal{S}_*^h inherit their values from the molecular dynamics. Therefore, in the spirit of mortar methods, we call the finite-element space \mathcal{S}^h the slave space and the approximation space spanned by the Shepard functions the master space.

Let us now describe, how to obtain the discrete representation of our transfer operator. Inserting $w = \sum_{\alpha \in \mathcal{A}} q_\alpha \varphi_\alpha$ and $\pi^h(w) = \sum_{p \in \mathcal{N}_*^h} \pi_p \lambda_p$ into (12), we obtain

$$M\pi = Rq \quad (16)$$

with $M = (m_{ts})_{t,s \in \mathcal{N}_*^h}$ and $R = (r_{s\alpha})_{s \in \mathcal{N}_*^h, \alpha \in \mathcal{A}}$ and

$$r_{s\alpha} = \int_{\Omega} \mu_s \varphi_\alpha \quad \text{and} \quad m_{ts} = \int_{\Omega} \lambda_t \mu_s. \quad (17)$$

here, we have set $q = (q_\alpha)_{\alpha \in \mathcal{A}}$ and $\pi = (\pi_p)_{p \in \mathcal{N}_*^h}$. This gives rise to our weak coupling operator in its algebraic representation

$$W = M^{-1}R, \quad (18)$$

which transfers the low-frequency information from the micro-scale to the macro-scale. We remark that this approach shows similarities to the bridging domain method. More precisely, the constraints in [7] in algebraic structure are given by

$$N\bar{w} = I_{\mathbb{R}^{d|\mathcal{A}| \times |\mathcal{A}|}} q \quad (19)$$

with N being the matrix containing the values of the FE shape functions evaluated at the atomic positions. Comparing (16) and (19) one can see, that in the bridging domain method, the fine scale (slave side) inherits the values from the coarse scale (master side), whereas in (16) the coarse scale (slave side) inherits the values from the fine scale (master side). Additionally, the weights in (19) are computed on a completely local basis, whereas in the weights in (16) are computed by means of local averaging. For a related approach in the context of multigrid methods we refer to [41] and the references cited therein.

Due to the definition of \mathcal{S}_*^h and for suitably chosen M^h , the matrix M has the character of a finite element mass matrix, is well conditioned and $M^{-1}\mu$ can be computed easily for any $\mu \in M^h$. For assembling the matrix R , we need to evaluate integrals of the form

$$\int_{\omega_\alpha \cap \text{supp}(\lambda_p)} \mu_p \varphi_\alpha dx. \quad (20)$$

In order to compute these integrals, the cut between the support of μ_p and the patch ω_α has to be computed. On the resulting polytope, then the quadrature has to be carried out. Since, following our approach, the cut polytopes can be controlled in their size but not in their shape, the quadrature is a challenging task. In order to deal with this problem we have developed and implemented the library `CUTLIB`, which allows for cut detection and quadrature on the resulting cut-polytopes; for details we refer to [42].

By construction, our coupling operator π^h allows for the decomposition of the kinetic energy T into a coarse scale and a fine scale part in an L^2 sense, analogue to [11]. In the case $M^h = \mathcal{S}_*^h$ which is known as the standard multiplier space in the mortar setting, we moreover have

$$\begin{aligned} T &= \frac{1}{2}(\dot{w}, \dot{w})_{L^2(\Omega')} \\ &= \frac{1}{2}(\dot{w}, \dot{\bar{w}})_{L^2(\Omega')} + \frac{1}{2}(\dot{w}, \dot{w}')_{L^2(\Omega')} \\ &= \frac{1}{2}(\dot{\bar{w}}, \dot{\bar{w}})_{L^2(\Omega')} + \frac{1}{2}(\dot{w}', \dot{\bar{w}})_{L^2(\Omega')} + \frac{1}{2}(\dot{w}, (I - \pi^h)\dot{w})_{L^2(\Omega')} \\ &= \frac{1}{2}(\dot{\bar{w}}, \dot{\bar{w}})_{L^2(\Omega')} + \frac{1}{2}(\dot{w}, (I - \pi^h)\dot{w})_{L^2(\Omega')} \end{aligned}$$

since the mixed term $\frac{1}{2}(\dot{w}', \dot{\bar{w}})_{L^2(\Omega')}$ vanishes due to the fact that $\text{range}(I - \pi^h) \perp M^h$.

Relation to the Bridging Scale Method In contrast to (18), the coarse scale description in the Bridging Scale Method [11] is given by

$$\widetilde{W} = M_{\text{con}}^{-1} N^T M_A, \quad (21)$$

with $M_{\text{con}} = N^T M_A N$ and M_A given by (2). In the Bridging Scale Method, the transition from coarse to fine scale is defined by interpolation and the projection from fine to coarse is defined as the least squares approximation of the atomistic displacements with respect to the atomistic mass matrix M_A . More precisely, the components of $M_{\text{con}} = \tilde{m}_{p,q \in \mathcal{N}^h}$ are given by

$$m_{pq}^S = \sum_{\alpha \in \mathcal{A}} m_\alpha \lambda_p(X_\alpha) \lambda_q(X_\alpha) = \sum_{\alpha \in \mathcal{A}} \frac{m_\alpha}{\text{meas}(\omega_\alpha)} \lambda_p(X_\alpha) \lambda_q(X_\alpha) \cdot \text{meas}(\omega_\alpha) \approx \int_{\Omega'} \lambda_p \lambda_q \, dx. \quad (22)$$

Thus, assuming that the density $\frac{m_\alpha}{\text{meas}(\omega_\alpha)}$ is one and that the patches $(\omega_\alpha)_{\alpha \in \mathcal{A}}$ fulfill $\omega_\alpha \cap \omega_\beta = \emptyset \iff \alpha \neq \beta$, (22) can be interpreted as a summed quadrature rule.

By introducing the scalar product $\langle \cdot, \cdot \rangle_{\text{BS}} := \langle M_A \cdot, \cdot \rangle$ on $\mathbb{R}^{|\mathcal{A}|} \times \mathbb{R}^{|\mathcal{A}|}$ the projection from the total displacement field w to the coarse part \bar{w} is given by

$$\langle N\bar{w}, N\mu \rangle_{\text{BS}} = \langle w, N\mu \rangle_{\text{BS}} \quad \forall \mu \in \mathbb{R}^{|\mathcal{N}_*^h|},$$

i.e., the bridging scale method can be seen to be based on the choice $\tilde{M}^h = \text{span}\{\lambda_p \mid p \in \mathcal{N}_*^h\}$. However, the coupling itself uses the discrete scalar product $\langle \cdot, \cdot \rangle_{\text{BS}}$, which distinguishes it from our approach, where the L^2 -scalar product connected to the coarse scale is used. This probably seems to be the more natural approach within the weak formulation of the finite element method.

For investigating the structure of the bridging scale operator \tilde{W} in more detail, let us consider the case that the masses of the atoms are equal, i.e., $m = m_1 = m_2 = \dots = m_{|\mathcal{A}|}$. Then, the atomistic mass matrix M_A reduces to $M_A = m \text{Id}$ and the coarse scale mass matrix becomes $M_{\text{con}} = N^T M_A N = m N^T N$. Thus, the operator \tilde{W} reduces to

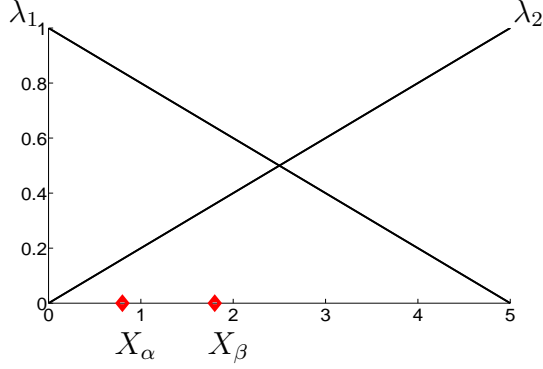
$$\tilde{W} = (N^T N)^{-1} N^T,$$

which are simply the normal equations stemming from $\langle N\bar{w} - w, N\mu \rangle \mu \in \mathbb{R}^{|\mathcal{N}_*^h|}$.

We now want to explore more differences and commonalities between (21) and (18). For sake of simplicity, we consider the case, that only two particles x_α and x_β are in the support of two shape functions ψ_1 and ψ_2 . Then the matrix N in (21) as well as the matrix R in (18) become quadratic.

$$N = \begin{pmatrix} \lambda_1(x_\alpha) & \lambda_1(x_\beta) \\ \lambda_2(x_\alpha) & \lambda_2(x_\beta) \end{pmatrix} \quad R = \begin{pmatrix} \int_{\omega_{1\alpha}} \lambda_1 \varphi_\alpha & \int_{\omega_{1\beta}} \lambda_1 \varphi_\beta \\ \int_{\omega_{2\alpha}} \lambda_2 \varphi_\alpha & \int_{\omega_{2\beta}} \lambda_2 \varphi_\beta \end{pmatrix}.$$

In the forthcoming, we consider the condition numbers $\kappa(\tilde{W})$ and $\kappa(W)$ in dependence of the distance $d_{\alpha\beta} := |X_\alpha - X_\beta|$. The condition number is indicative of the stability or sensitivity of the transfer operators. In Table 1, the condition number in dependence of the distance is shown. It can be seen that the condition number $\kappa(\tilde{W})$ is increasing while $\kappa(W)$ show a very slow growth. In fact, the growth of the condition number of the matrix R can be controlled, since the integration domains ω can be chosen individually to fulfill $\omega_{1\alpha} \neq \omega_{2\alpha} \neq \omega_{1\beta} \neq \omega_{2\beta}$. Obviously, the argumentation above also holds for the case of more than two particles in the support of the element.


 Figure 6: *Two particles in the support of one element*

$d_{\alpha\beta}$	1	0.9	0.8	0.7	0.6	0.5	0.4	0.3
$\kappa(\widetilde{W})$	6.1905	6.9812	7.9746	9.2577	10.9756	13.3893	17.0212	23.0900
$\kappa(W)$	3.1027	3.2188	3.3274	3.4186	3.5502	3.6052	3.6559	3.7311

 Table 1: *Comparison of the condition number of N and W w.r.t. the distance between the two particles α and β*

5 Numerical Results

5.1 A One Dimensional Example

We adopt the numerical example of [12]: The interval $[-100r_{\text{EQ}}, 100r_{\text{EQ}}]$ is covered by 40 linear finite elements with mesh size $h = 5r_{\text{EQ}}$. To each of the 56 atoms between $-28r_{\text{EQ}}$ and $28r_{\text{EQ}}$, a patch of size $0.6r_{\text{EQ}}$ is attached. For the molecular scale the Lennard-Jones (LJ) potential is given by

$$V_{\text{LJ}}(r) = 4\varepsilon \left(\frac{\sigma^{12}}{r^{12}} - \frac{\sigma^6}{r^6} \right); \quad \sigma = 1, \varepsilon = 1. \quad (23)$$

The equilibrium state of the molecules is given by $r_{\text{EQ}} = 2^{1/6}\sigma$. Outside the MD/FE region the nodal forces are calculated via the Cauchy-Born rule. The Cauchy Born rule states that the atomic system deforms according to the continuum deformation gradient F . More precisely let r_{ij}^{sp} (r_{ij}^{ref}) be the position of atom i in the spatial (reference) configuration. Then the distance of the particles in their spatial (reference) configuration is given by

$$r_{ij}^{(*)} = r_i^{(*)} - r_j^{(*)} \quad * = \{\text{sp}, \text{ref}\}.$$

In the Cauchy-Born rule setting it is assumed that the spatial configuration results from the application of the local deformation gradient $F = \nabla\phi$ to the reference configuration,

i.e.

$$r_{ij}^{\text{sp}} = F \cdot r_{ij}^{\text{ref}}.$$

Let us note that the the Cauchy-Born rule fails for sufficiently large deformations [43]. The initial amplitude in the molecular part is given by

$$u(r) = 0.12 \cdot \frac{e^{(-r/\sigma)^2} - u_c}{1 - u_c} \left(1 + 0.1 \cdot \cos \left(\frac{8\pi}{5} r \right) \right) \quad \text{with } u_c = e^{-(1/5)^2},$$

i.e. the amplitude of the wave was 12% of the equilibrium spacing.

Let T_{end} be the total run time of the simulation. We follow [12] by advancing both simulations by a time step $\tau \in [0, T]$. Thus in a single time step the coarse scale simulation is advanced once and the fine scale simulation is advanced m times. The fractional time steps in the n -th coarse scale time step is given by $[j] := n + \frac{j}{m}$ and the sub cycle time step is given by $\tau_m = \frac{\tau}{m}$. On the fine scale the velocity Verlet and on the coarse scale the explicit central difference algorithm are used. We furthermore assume that p^n, q^n, s^n are given, then the update is given by:

$$\begin{aligned} p^{[j+1]} &= p^{[j]} + q^{[j]} \tau_m + 1/2 s^{[j]} \tau_m^2 & p \text{ MD displacement} \\ q^{[j+1/2]} &= q^{[j]} + s^{[j]} \tau_m & q \text{ MD velocity} \\ s^{[j+1]} &= M_A^{-1} f(p^{[j+1]}) & s \text{ MD acceleration} \\ q^{[j+1]} &= q^{[j+1/2]} + \frac{1}{2} s^{[j+1]} \tau_m. \end{aligned}$$

After $m = 50$ fine scale steps the molecular dynamics quantities of the coarse time step $n + 1$ are obtained. In order to advance the coarse scale simulation from n to $n + 1$ the internal forces are computed by combining the coarse scale displacement \bar{w} and the fine scale part $Q = (I - NW)$ of the molecular simulation.

$$\begin{aligned} d^{n+1} &= d^n + v^n \tau + \frac{1}{2} a^n \tau^2 & d \text{ FE displacement} \\ a^{n+1} &= M^{-1} N^T f(Nd + Qq) & a \text{ FE acceleration} \\ v^{n+1} &= v^n + \frac{1}{2} (a^n + a^{n+1}) \tau & v \text{ FE velocity.} \end{aligned}$$

In our simulation we chose $\tau = 0.2$.

In Figure 7, the coupled MD/FE simulation with the multiplier space M^h is shown. The square-marked line (red) represents the displacements of the fine scale. The continuous line (blue) maps the displacement of the coarse displacement. For comparison to the multiscale simulation a full atomistic simulation using 420 atoms is shown in Figure 8. The performance of the modified multiplier space M_{mod}^h for the same problem is shown in Figure 9.

As can be seen by comparing Figure 7 with Figure 9, there are only slight differences for the choices M^h and M_{mod}^h . We expect a different behaviour in higher dimensions.

In the following, we compare our new weak transfer operator with the transfer operator \widetilde{W} . As measures for the comparison we chose the norms $\| \cdot \|_{L^2(\Omega)}$ and $\| \cdot \|_{\infty}$.

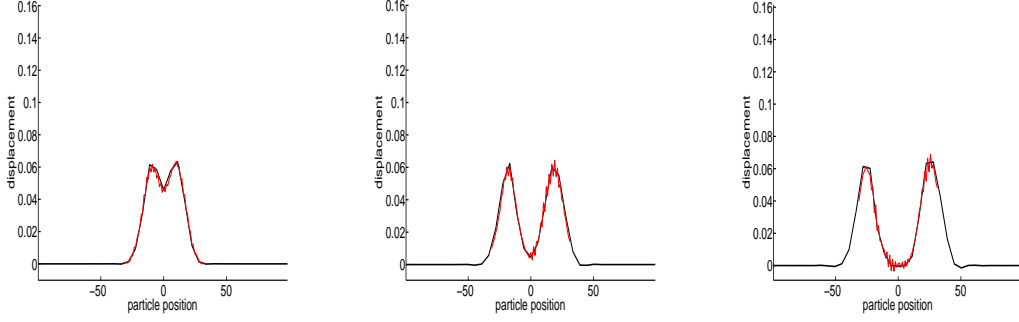


Figure 7: *FE-MD simulation using M^h as multiplier space, for the coarse scale time steps $n = 3, n = 12$ and $n = 18$.*

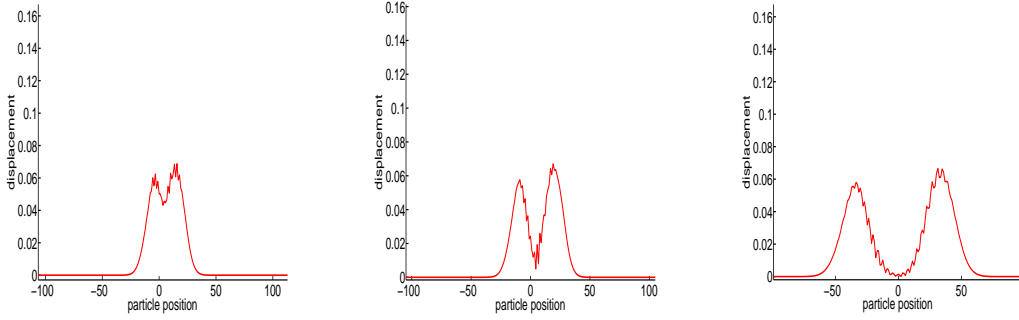


Figure 8: *Full MD simulation, for the fine scale time steps: $m \cdot n = 150, 600$ and 900*

In order to measure the difference between the discrete displacement field stemming from the atomistic scale with the values of the coarse scale, in our approach we choose the the L^2 norm. On Ω' , this error can easily be computed as

$$\|w - k_i(w)\|_{L^2(\Omega')}^2 = w^T M_{\text{PUM}} w - 2w^T R k_i(w) + k_i(w)^T M k_i(w), \quad i = 1, 2, \quad (24)$$

where M_{PUM} is the PUM mass matrix whose elements are given by $m_{\alpha\beta}^{\text{PUM}} = \int \varphi_\alpha \varphi_\beta$. Here, k_1 is the Least Squares projection \widetilde{W} and k_2 is the weak coupling operator W . For the error in the $\|\cdot\|_\infty$ norm, we simply computed

$$\|w - N(k_i(w))\|_\infty^2, \quad i = 1, 2, \quad (25)$$

The following table shows the obtained errors for $i = 1, 2$.

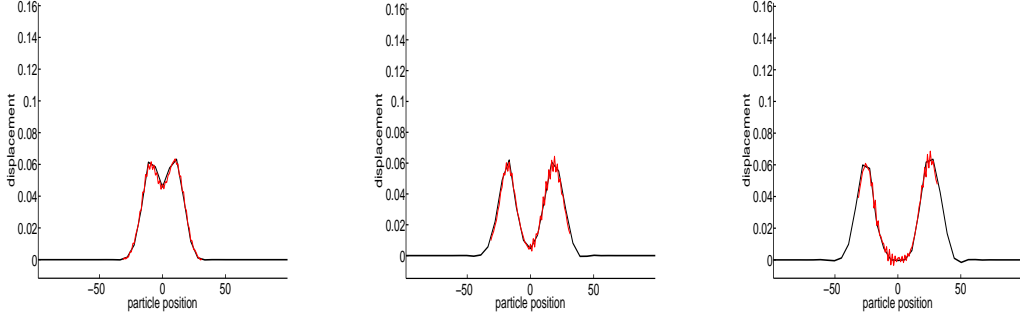


Figure 9: *FE-MD simulation using M_{mod}^h as multiplier space , for the coarse scale time steps $n = 3, n = 12$ and $n = 18$*

coarse time step	$\ \cdot \ _{L^2(\Omega')}$		$\ \cdot \ _{\infty}$	
	bridging scale	weak coupling	bridging scale	weak coupling
3	$6.0 \cdot 10^{-3}$	$2.7 \cdot 10^{-4}$	$2.8 \cdot 10^{-2}$	$6.7 \cdot 10^{-3}$
6	$3.0 \cdot 10^{-2}$	$1.1 \cdot 10^{-4}$	$5.3 \cdot 10^{-2}$	$4.8 \cdot 10^{-3}$
9	$6.0 \cdot 10^{-2}$	$5.7 \cdot 10^{-4}$	$7.5 \cdot 10^{-2}$	$4.8 \cdot 10^{-3}$
12	$8.1 \cdot 10^{-2}$	$1.2 \cdot 10^{-3}$	$7.3 \cdot 10^{-2}$	$3.9 \cdot 10^{-3}$
15	$8.3 \cdot 10^{-2}$	$2.3 \cdot 10^{-3}$	$7.4 \cdot 10^{-2}$	$6.1 \cdot 10^{-3}$
18	$7.5 \cdot 10^{-2}$	$2.1 \cdot 10^{-3}$	$7.3 \cdot 10^{-2}$	$5.1 \cdot 10^{-3}$

Table 2: *Difference between the discrete displacement field stemming from the atomistic scale with the values of the coarse scale in the $\| \cdot \|_{L^2(\Omega')}$ - and $\| \cdot \|_{\infty}$ norm*

5.2 A Two Dimensional Example

In this example, we test the performance of our projection operator π^h for $d = 2$. To do so, we study wave propagation through a small sheet. Considering the domain $\Omega = [0, 80] \times [400, 800] \subset \mathbb{R}^2$ the coupling region chosen is $\Omega' = [0, 80] \times [400, 550] \subset \Omega$. An initial displacement in the molecular domain Ω' propagates out of the coupling zone into $\Omega \setminus \Omega'$, where only coarse finite elements are used. The following picture is a sketch of the simulation geometry:

The initial displacement in Ω' is a combination of high- and low frequency parts:

$$u(x, y) = \frac{A}{A - u_c} (Ae^{-(y-t)/\sigma} - u_c) \left(1 + b \cos \left(\frac{2\pi}{H}(y - t) \right) \right) e_y$$

with $e_y = (0, 1)^T$, $t = 510$, $\sigma = 15$, $H = \sigma/4$, $A = 0.15$, $b = 0.3$, $r_c = 5 \cdot \sigma$ and $u_c = Ae^{(r_c/\sigma)^2}$, where we adopted the notation used in [12].

The potential function is the LJ-Potential (23) with nearest-neighbour interaction, i.e $r_{cut} = 3/2 \cdot r_{req}$. For the coarse scale we employ standard linear elastic Saint-Venant

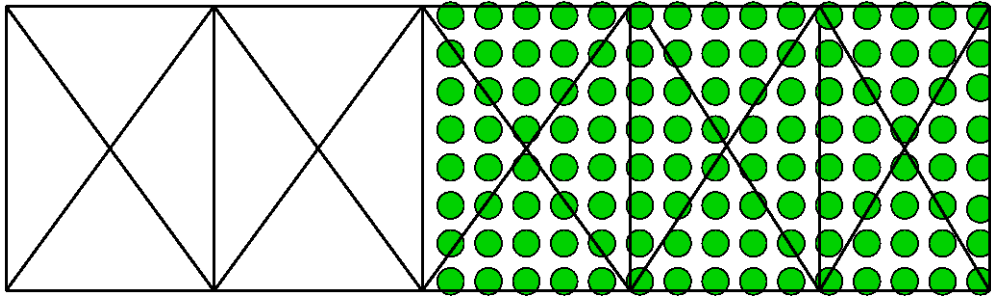


Figure 10: A sketch of the computational domain in 2d

material law with elastic module $E = 30$ and Poisson ratio $\nu = 0.2589$, discretized on a triangular mesh.

The coupling zone contained 11.130 atoms and about 585 triangles. The patch size is $h = 1.7$ for each atom. Since the focus here is put on the properties of the new transfer operator, the MD block was chosen large enough to avoid spurious reflections at the boundary.

For the integration in time, we have used the time-stepping scheme given in Subsection 5.1 with the following changes applied:

- The coarse-scale force is calculated by linear elasticity $F = F(d)$.
- The coupling is done by overwriting the coarse-scale displacement and velocities in each time step in the coupling zone by the values obtained from the L^2 projection of the values on the fine scale.

We chose $\tau = 0.1$ and $m = 2$. Figure 11 shows the time-evolution of the absolute value of the perturbation as it propagates into the coarse region $\Omega \setminus \Omega'$. In the coupling region, only the atomic displacements are shown. It can be seen that by using the L^2 projection an almost seamless transition between the scales can be achieved.

6 Conclusion

We presented a new transfer operator on the basis of weighted local averaging instead of point wise taken values. The local weight functions are constructed by assigning a partition of unity to the molecular degrees of freedom. Consequently, the decomposition of the displacements into low frequency and high frequency can be realized by a weighted L^2 projection. We also showed that in our scheme the Bridging Scale method can be interpreted as a special case of this new coupling approach. In numerical experiments we compared the results of the coupled simulation with a full atomistic simulation and showed that obtained results are almost identical.

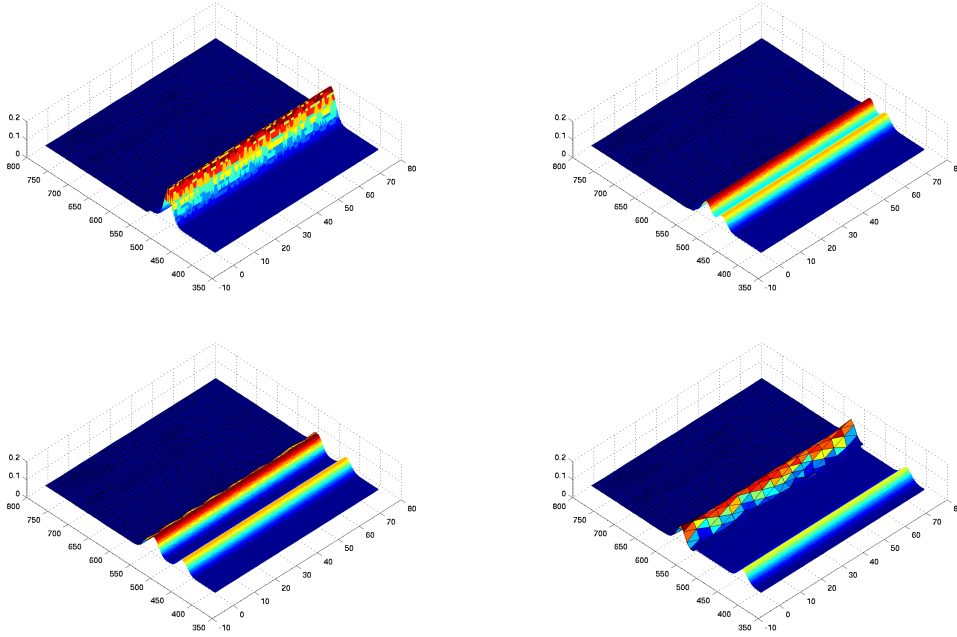


Figure 11: *FE-MD simulation using the weak transfer operator. Absolute value of the displacement after $n = 1$, $n = 30$, $n = 55$ and $n = 100$ time steps.*

Acknowledgments

This work was supported by the Deutsche Forschungsgemeinschaft through the SFB 611 “Singular Phenomena and Scaling in Mathematical Models”. The authors would like to thank Dorian Krause for his help and the fruitful discussions and the anonymous referees for their remarks and suggestions.

References

- [1] E. Tadmor, M. Ortiz, and R. Phillips. Quasicontinuum analysis of defects in solids. *Phil. Mag. A*, 73:1529–1563, 1996.
- [2] P.G. Kevrekidis, I.G. Kevrekidis, A.R. Bishop, and E.S. Titi. Continuum approach to discreteness. *Phys. Rev. E*, 65(4):046613, 2002.
- [3] W.E and Z. Huang. A dynamic atomistic-continuum method for the simulation of crystalline materials. *J. Comput. Phys.*, 182(1):234–261, 2002.
- [4] X.Blanc, C.LeBris, and P.Lions. From molecular models to continuum mechanics. *Arch. Ration. Mech. Anal.*, 164(4):341–381, 2002.
- [5] F.F.Abraham, J.Q. Broughton, N.Bernstein, and E.Kaxiras. Spanning the contin-

- uum to quantum length scales in a dynamic simulation of brittle fracture. *Europhys. Lett*, 44(6):783–787, 1998.
- [6] J. Knap and M. Ortiz. An analysis of the quasicontinuum method. *J. Mech. Phys. Solids*, 49(9):1899–1923, 2001.
- [7] S.P. Xiao and T. Belytschko. A bridging domain method for coupling continua with molecular dynamics. *Comp. Meth. Appl. Mech. Engrg.*, 193:1645–1669, 2004.
- [8] T. Belytschko and S.P. Xiao. Coupling methods for continuum model with molecular model. *Int. J. f. Multisc. Comp. Eng*, 1(1):115–126, 2003.
- [9] W.A. Curtin and R.E. Miller. Atomistic/continuum coupling in computational materials science. *Mod. Simul. Mater. Sci. Engrg.*, 11:R33–R68, 2003.
- [10] L.E. Shilkrot, W.A. Curtin, and R.E. Miller. A coupled atomistic/continuum model of defects in solids. *J. Mech. Phys.*, 50:2085–2106, 2002.
- [11] G.J. Wagner and W.K. Liu. Coupling of atomistic and continuum simulations using a bridging scale decomposition. *J. Comp. Phy.*, 190:1261–1289, 2003.
- [12] W.K. Liu, E.G. Karpov, and H.S. Park. *Nano Mechanics and Materials*. Wiley, 2006.
- [13] S. Tang, T. Y. Hou, and W.K. Liu. A mathematical framework of the bridging scale method. *Int. J. Numer. Meth. Engrg.*, 65:1688–1713, 2005.
- [14] J. Fish, M.A. Nuggehally, M.S. Shepard, C.P. Picu, S. Badia, M.L. Parks, and M. Gunzburger. Concurrent AtC coupling based on a blend of the continuum stress and the atomistic force. *Comp. Meth. Appl. Mech. Engrg.*, 196:4548–4560, 2007.
- [15] M.A. Nuggehally, M.S. Shepard, C.P. Picu, and J. Fish. Adaptive model selection procedure for concurrent multiscale problems. *Int. J. Mult. Comp. Engrg*, 5:369–386, 2007.
- [16] S. Badia, M. Parks, P. Bochev, M. Gunzburger, and R. Lehoucq. On atomistic-to-continuum coupling by blending. *SIAM Multiscale Modeling Simulation*, 7(1):381–406, 2008.
- [17] S.A. Adelman and J.D. Doll. Generalized Langevin equations for atom/solid-surface scattering: General formulation for classical scattering off harmonic solids. *J. Chem. Phys.*, 64(4):2375–2388, 1976.
- [18] D. Givoli. Non-reflecting boundary conditions. *J. Comp. Phy.*, 94:1–29, 1991.
- [19] W. Cai, M. DeKoning, V.V. Bulatov, and S. Yip. Minimizing boundary reflection in coupled-domain simulations. *Phys. Rev. Lett.*, 85:3213–3216, 2000.

- [20] J.P. Berenger. A perfectly matched layer for the absorption of electromagnetic waves. *J. Comp. Phy*, 114:185–200, 1994.
- [21] A.C. To and S. Li. Perfectly matched multiscale simulation. *Phy Rev. B*, 72:035414–1 – 8, 2005.
- [22] G.J. Wagner and W.K. Liu. Hierarchical enrichment for bridging scales and mesh-free boundary conditions. *Int. J. Num. Meth. Engng*, 50:507–524, 2001.
- [23] T. Dickopf and R. Krause. Efficient simulation of multi-body contact problems on complex geometries: A flexible decomposition approach using constrained minimization. *to appear*, 2007.
- [24] P.G. Ciarlet. *Mathematical Elasticity; Volume 1: Three Dimensional Elasticity*. North-Holland, Amsterdam, 1988.
- [25] T. Hughes, G. Feijoo, J. Mazzei, and J. Quincy. The variational multiscale method - a paradigm for computational mechanics. *Comput. Meth. Appl. Mech.*, 166:3–24, 1998.
- [26] J. Broughton, F. Abraham, N. Bernstein, and E. Kaxiras. Concurrent coupling of length scales: methodology and application. *Phys. Rev. B*, 60:2391–2403, 1999.
- [27] C. Bernardi, Y. Maday, and A.T. Patera. A new nonconforming approach to domain decomposition: The mortar element method. In H. Brezis et al., editor, *Nonlinear partial differential equations and their applications. Collège de France Seminar, volume XI. Lectures presented at the weekly seminar on applied mathematics*, 299, pages 13–51. Harlow: Longman, scientific & technical pitman res. notes math. edition, 1994.
- [28] F. Ben Belgacem. The mortar finite element method with lagrange multipliers. *Numer. Math.*, 84(2):173–197, 1999.
- [29] R. Krause. *Monotone Multigrid Methods for Signorini’s Problem with Friction*. PhD thesis, Freie Universität Berlin, 2001.
- [30] I. Babuska and J.M. Melenk. The partition of unity method. *Int. J. Numer. Meth. Engrg.*, 40:727–758, 1997.
- [31] M. Griebel and M. A. Schweitzer. A Particle-Partition of Unity Method for the solution of Elliptic, Parabolic and Hyperbolic PDE. *SIAM J. Sci. Comp.*, 22(3):853–890, 2000.
- [32] M. A. Schweitzer. *A Parallel Multilevel Partition of Unity Method for Elliptic Partial Differential Equations*. Number 29 in LNCSE. Springer, 2003.
- [33] D. Shepard. A two-dimensional function for irregularly spaced data. In *ACM National Conference*, pages 517–524, 1968.

- [34] P. Lancaster and K. Salkauskas. Surfaces generated by moving least squares method. *Math. Comp*, 27:141–158, 1981.
- [35] J.S. Chen, C. Pan, and C.I. Wu. Large deformation analysis of rubber based on a reproducing kernel particle method. *Comp. Mech.*, 19:211–227, 1997.
- [36] W.K. Liu, S. Jun, S. Li, J. Adee, and T. Belytschko. Reproducing kernel particle methods for structural mechanics. *Int. J. Numer. Methods Engrg.*, 38:1655–1679, 1995.
- [37] W.K. Liu, S. Jun, and Y.F. Zhang. Reproducing kernel particle methods. *Int. J. Numer. Meth. Fluids*, 20:1081–1106, 1995.
- [38] H. Wendland. Piecewise polynomial, positive definite and compactly supported radial functions of minimal degree. *Adv. in Comput. Math.*, 4:389–396, 1995.
- [39] Z. Wu. Compactly supported positive definite radial functions. *Adv. in Comput. Math.*, 4:283–292, 1995.
- [40] A. Quarteroni and A. Valli. *Domain Decomposition Methods for Partial Differential Equations*. Oxford Science Publications, 1999.
- [41] L. R. Scott and S. Zhang. Higher-dimensional nonnested multigrid methods. *Math. Comp.*, 58(198):457–466, 1992.
- [42] K. Fackeldey, D. Krause, and R. Krause. Concepts and implementation of the weak coupling method. in preparation.
- [43] G. Friesecke and F. Theil. Validity and failure of the cauchy-born hypothesis in a two-dimensional mass-spring lattice. *J. Nonlinear Sci.*, 12:445–478, 2002.
- [44] M. Zhou and D.L. McDowell. Equivalent continuum for dynamically deforming atomistic particle systems. *Phil. Mag. A*, 82(13):2547–2574, 2002.
- [45] E. B. Webb, J. A. Zimmerman, and S. C. Seel. Reconsideration of continuum thermomechanical quantities in atomic scale simulations. *Math. Mech. of Solids*, 13(3-4):221–266, 2008.
- [46] M. Gullett, M. F. Horstemeyer, M. I. Baskes, and H. Fang. A deformation gradient tensor and strain tensors for atomistic simulations. *Modelling Simul. Mater. Sci. Engrg.*, 16:015001 (17pp), 2008.